17th World Conference on Earthquake Engineering, 17WCEE
Sendai, Japan - September 13th to 18th 2020

INFLUENCES OF GROUNDWATER LEVEL ON INSTABILITY OF RESIDENCES ON COHESIVE SOILS UNDER EARTHQUAKES

Kazuya Yasuhara[(1)], Kaoru Kobayashi [(2)], Daisuke Kazumi [(3)] and Baba, T.[(4)]

[(1)] Professor Emeritus, *ICAS Ibaraki University, 2-1-1 Bunkyo, Mito, 310-8512, Ibaraki, Japan kazuya.yasuhara.0927@vc.ibaraki.ac.jp*

[(2)] *Professor, Ibaraki University, Hitachi, Ibaraki, Japan*
[(3)] *Engineer, Fukushima Prefecture, Fukushima, Japan*
[(4)] *Chief Engineer, Seico Consultant Co. Ltd., Kurume, Fukuoka, Japan*

Abstract

Results of cyclic and post-cyclic triaxial tests of undisturbed volcanic cohesive soils taken from a damage site were used with the Newmark method to investigate the influences of groundwater level (GWL) on residual deformation. The putative cause of severe damage to residences in Mashiki Town, Kumamoto, Japan, which was stricken by the great earthquakes in 2016, was related to GWL.

The following were concluded from the investigation described above.

i) An influential degree of GWL affecting post-earthquake residual deformation was associated with the slope failure circle extending to embankments or foundation ground. Devastating damage to residences in Mashiki Town was probably caused by the large circle failure passing the bottoms of foundations beneath residential embankments.

ii) To avoid the complete collapse of residences at Mashiki Town during earthquakes, GWL should be lowered to around 7 m from the embankment surface. After doing so, damage would be limited to partial failure of residences, not complete failure.

iii) A level of GWL of 4.0 m from the surface existed at the moment the main shock struck in Mashiki Town. That high GWL was critically important for causing increased damage, judging from both the amount of settlement and the angle of inclination of residences.

iv) The findings stated above emphasize that monitoring GWL in this area is an important proactive measure for reduction of earthquake-induced residual deformation of embankments and foundations.

KEYWORDS Groundwater level, Kumamoto earthquake, Residual deformation, Residence, Newmark method, Volcanic-ash cohesive soils

1. Introduction

A Mj6.5 earthquake shook Kumamoto prefecture in Japan on April 14, 2016. Soon thereafter, on April 16, a Mj7.3 earthquake struck Kumamoto and Oita prefectures. A recent investigation by Yoshimi et al. [1] revealed that nonlinearity of the seismic response of deposits comprising layered volcanic ash cohesive soils and pumice exacerbated the devastating damage to residences of Mashiki town near Kumamoto city during the earthquake. Based on those findings, the authors hypothesized that nonlinearity of seismic response for soft deposits is associated with the cyclic degradation of strength and stiffness in deposits of cohesive volcanic ash soils, which severely damaged residences. Using the methodology proposed by Yasuhara et al. [2,3] from earlier studies of degradation characteristics of cohesive soils, the authors attempted to predict the residential settlement and lateral deformation of cohesive volcanic ash soils causing such severe destruction in residential areas [4, 5].

Drastic residual deformation caused by earthquakes is the main reason for devastating damage to infrastructure and residences that occurs during and after successive earthquakes. The damage to residences in Mashiki Town during the Kumamoto earthquake was putatively influenced by groundwater level (GWL) to some degree.

Results of cyclic and post-cyclic triaxial tests of undisturbed volcanic cohesive soils taken from the damage site were used with the Newmark method to investigate GWL effects on residual deformation, which probably led to severe damage to residences in Mashiki Town.

2. Residential Site Damage Features

The devastation in the aftermath of the 2016 Kumamoto earthquake included 8336 complete residential failures. Examples of the damaged residences and retaining walls are shown respectively in Photo 1 and Fig. 1. From a geotechnical perspective, the authors inferred at least two reasons underlying such severe earthquake damage to residences and retaining walls.

(i) Soil embankments used as residential foundations lost strength and stiffness, engendering their collapse, severe settlement, and deformation [4][5].

(ii) Predominant nonlinearity and amplification of the ground motion degraded the stiffness and strength of volcanic ash cohesive soils, leading to greater degrees of lateral displacement [1].

Reason (ii) above was inferred as the mechanism damaging embankments and residences by rocking motions of residences and retaining walls. The damage was attributable to earthquake-induced degradation and decreased strength and stiffness of foundation soils of residences and backfill soils of retaining walls [4].

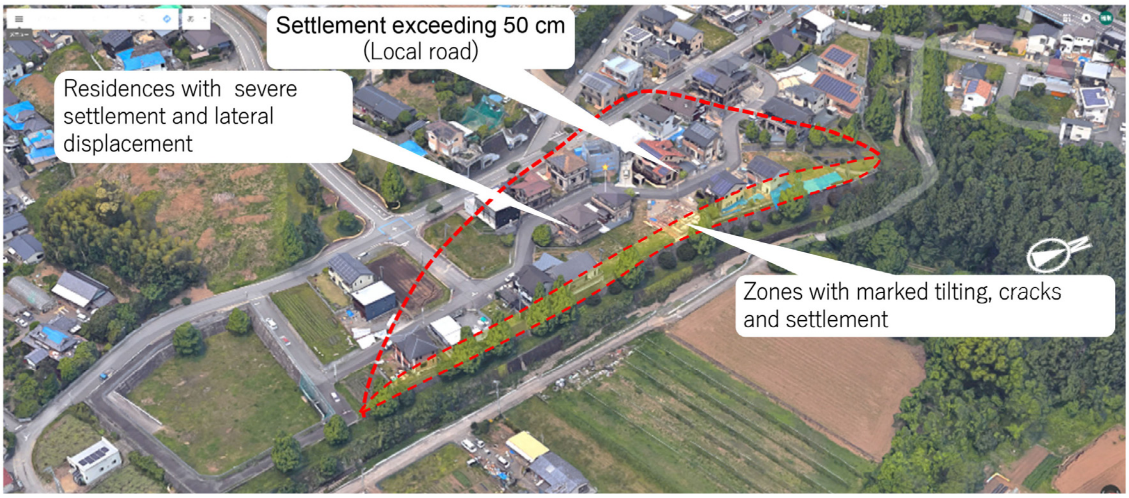

Photo 1 – Example of damage features in residential areas [6]

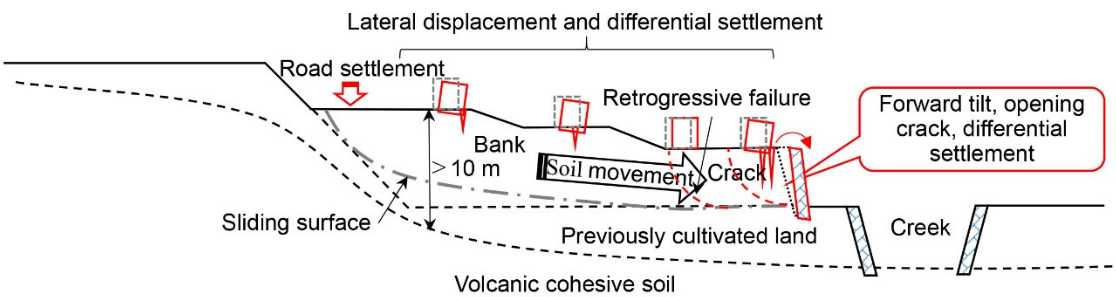

Fig. 1 – Key sketch of a damaged embankment for residences [6]

3. Subsoil Conditions and Index Properties

3.1 Subsoil conditions at the site

A site investigation was conducted by AIST after the Kumamoto earthquake in the Miyazono district of Mashiki town in Kumamoto, which exhibited the greatest damage. It has deposits of soft volcanic ash cohesive soils covered by a loam layer and an embankment.

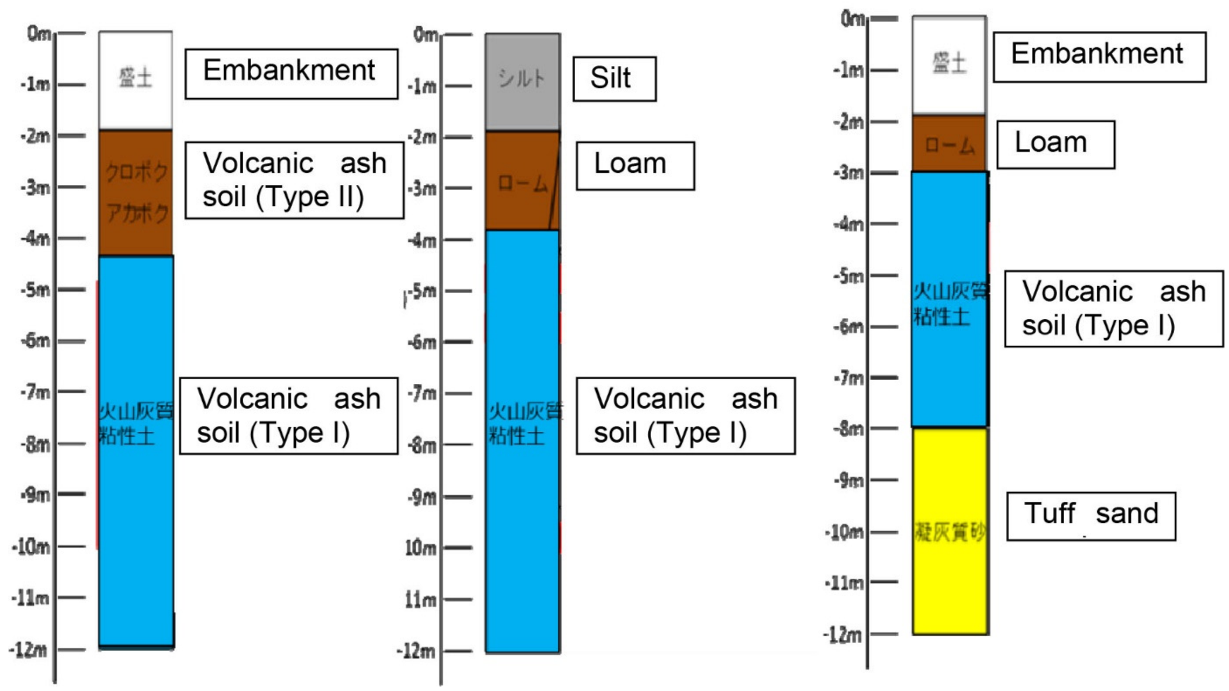

Fig. 2 – Soil profile of samples taken from the damage site

3.2 Index properties of volcanic-ash cohesive soils

Before dynamic triaxial shear deformation tests and post-cyclic monotonic triaxial tests at the laboratory, index tests were conducted of two kinds of volcanic ash cohesive soils obtained at the site.

Table 1 – Index properties of soils used for tests

	Volcanic ash cohesive soil (I-type)	Volcanic ash cohesive soil (II-type)
Density of soil particle, ρ_s (t/m^3)	2.731	2.475.
Initial water content, w_0 (%)	63.9	101
Liquid limit, w_L (%)	61.1	113.9
Plasticity index, I_p	19.7	39.2
Fine grain particle content, F_c (%)	60.6	73.8
Soil classification	VH_1	VH1-S or MHS-G

According to results from both index tests, representatively demonstrating that ρ_s = 2.756–2.771 t/m^3, w_i = 63.3% – 74.2%, and I_p = 31.1–35.0, soil specimens were classified as compressible silt-rich (approximately 50%) cohesive soils (VH$_1$-S or MHS-G) with low strength [5]. Those are recognized respectively from plastic charts and grain size distribution curves [5]. Therefore, we inferred that these volcanic-ash cohesive soils are related to the severe residential damage occurring in Mashiki town during the earthquakes.

4. Triaxial Testing Scheme

Tables 2 and 3 present the conditions of post-cyclic undrained triaxial compression tests on undisturbed volcanic cohesive soil cylindrical specimens of 5 cm diameter and 10 cm length.

Table 2 – Cyclic triaxial testing conditions (Series I and Series II)

Sample name	Sample no.	Effective confining pressure σ_c'(kN/m^2)	Cyclic test					Monotonic loading test	Ref. (test series)
			Cyclic stress ratio $(\sigma_a$-$\sigma_r)/2\sigma_c$'	Loading frequency f (Hz)	No. of load cycles N (回)	Aimed excess pore pressure ratio $\Delta u_{cy}/\sigma_c$'	Double amplitude strain ε_{DA} (%)	Axial strain rate (%/min)	
T3-1	T3-1-1	65	0.30	0.1	14	0.6	—	0.1	I
T3-2	T3-2-1	75	0.25		6	0.4			
	T3-2-2		0.30		24	0.9			
	T3-2-3		0.35		3	0.5			
T3-3	T3-3-1	90	0.25		58	0.7			
	T3-3-2		0.30		1	0.3			
	T3-3-3		0.35		21	0.8			
T4-1	T4-1-1	30	-	-	-	-	-		
	T4-1-2	60							
	T4-1-3	90							
T5-1	T5-1-1	100	0.373	0.1	3	—	1		II
	T5-1-2		0.373		11		3		
	T5-1-3		0.373		27		5		
	T5-1-4		0.373		57		7		
	T5-1-5		0.30		103		10		
	T5-1-6		0.35		55		10		
	T5-1-7		0.40		34		10		
	T5-1-8		0.45		23		10		
	T5-1-9	50	-	-	-	-	-		
	T5-1-10	100							
	T5-1-11	200							

This test scheme can be characterized as described below.

i) Cyclic stress ratio τ_{cy}/σ'_c of 0.25–0.35 and the number of load cycles from 1 through 58 were combined as testing conditions for Series I.

ii)

Table 3 – Cyclic triaxial testing conditions (Series III)

<table>
<tr><th>Sample name</th><th>Confining pressure
σ'_c(kN/m^2)</th><th>Cyclic stress ratio
$(\sigma_a\text{-}\sigma_r)/2\sigma'_c$</th><th>Frequency
f (Hz)</th><th>No. of load cycles
N (cycle)</th><th>Aimed excess pore pressure ratio
$\Delta u/\sigma'_c$</th><th>Aimed strain
ε_{DA} (%)</th><th>Monotonic strain rate
(%/min)</th></tr>
<tr><td>T6-4</td><td rowspan="9">100</td><td rowspan="5">0.427</td><td rowspan="9">0.1</td><td>3</td><td rowspan="9">—</td><td>1</td><td rowspan="9">0.1</td></tr>
<tr><td></td><td></td><td></td></tr>
<tr><td>T6-5</td><td>11</td><td>3</td></tr>
<tr><td>T6-6</td><td>27</td><td>5</td></tr>
<tr><td>T6-7</td><td>57</td><td>7</td></tr>
<tr><td>T6-8</td><td>0.332</td><td>—</td><td>10</td></tr>
<tr><td>T6-9</td><td>0.376</td><td>120</td><td>10</td></tr>
<tr><td>T6-10</td><td>0.404</td><td>115</td><td>10</td></tr>
<tr><td>T6-11</td><td>0.477</td><td>42</td><td>10</td></tr>
</table>

ii) The testing program in Series I is planned to combine the normalized cyclic shear stress τ_{cy}/σ'_c and the number of cycles to obtain widely various normalized excess pore pressure $\Delta u_{cy}/\sigma'_c$ of 0–1.0, as generated during undrained cyclic loading.

iii) The double amplitude axial strain ε_{DA} generated during undrained cycling in Series I is not large, but the maximum value of the normalized excess pore pressure becomes nearly 0.9.

iv) Double amplitude axial strain was varied with 1, 3, 5, 7, and 10% for Series II under constant cyclic shear stress ratio equal to cyclic strength of 0.373, as ascertained from the dynamic strength test results. This procedure is done following a testing method suitable for modified Newmark methods proposed by Tatsuoka et al. [7].

v) The confining pressure with 100 kPa and cyclic frequency with 0.1 Hz is the same as that used for Series I and Series II.

5. Test Results and Their Interpretation

5.1 Cyclic strength

The following procedures were proposed by the Japanese Geotechnical Society [8] to assess the shear modulus and shear strain relations. The cyclic strength curve was obtained in the form of cyclic shear stress vs. the number of load cycles as portrayed in Fig. 3 under stress controlled with 0.1 Hz frequency. The cyclic shear stress ratio,τ_{cy}/σ'_c, which is used for Newmark's method [9] for residual deformation prediction, was found to be 0.373 for Type-I soils and 0.423 for Type-II soils as RL_{20} from this result, corresponding to the load cycle N_{20} and the double amplitude axial strain ε_{DA} respectively equal to 20 and 5%.

On both soils, stress-controlled undrained triaxial compression tests were followed by undrained monotonic shearing, as shown in Table 1, using the stress ratio of 0.373 for Type-I soils and 0.423 for Type-II soils as the standard. The cyclic load was applied to each specimen until the prescribed double amplitude axial strains ε_{DA} of 1, 3, 7, and 10% were attained. Results show that the load number of cycles varied depending on the time at which each prescribed ε_{DA} was attained.

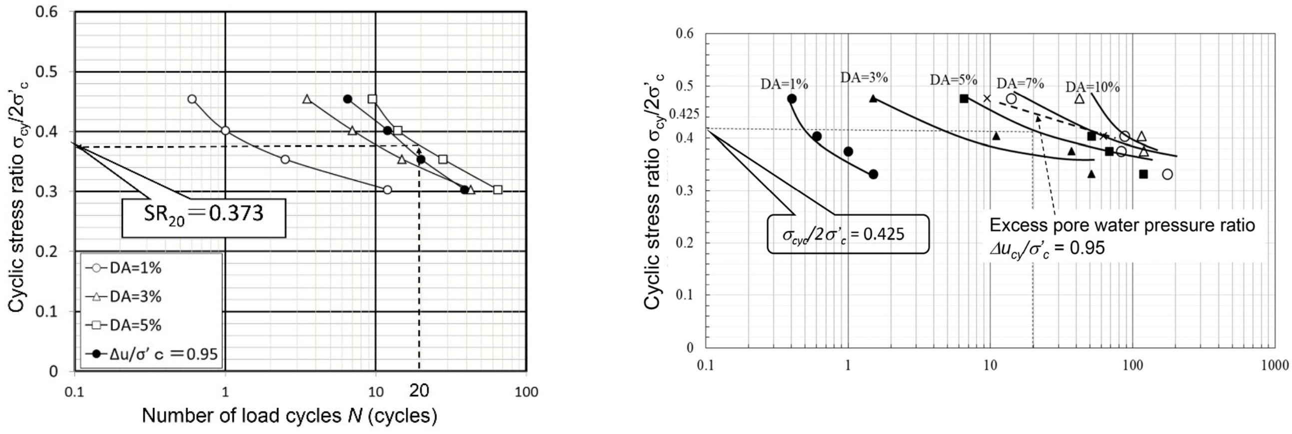

(a) I-type (b) II-type

Fig. 3 – Cyclic strengths of two type soil specimens

5.2 Post-cyclic performance

5.2.1 Post-cyclic stress–strain relations

Fig. 4 portrays stress vs. strain curves with and without undrained cyclic loading. The undrained strength was ascertained from half of the maximum principal stress difference, as $(\sigma_1\text{-}\sigma_3)_{max}/2$. The secant modulus was found from the gradient of the straight line passing through this coordinate and the point corresponding to half of the maximum principal stress difference, designated as $(\sigma_1\text{-}\sigma_3)_{max}/2$.

The test scheme is characterized as described below.

i) Cyclic stress ratio τ_{cy}/σ'_c of 0.25–0.35 and the number of load cycles from 1 through 58 were combined as testing conditions.

ii) The testing program is planned to combine the normalized cyclic shear stress τ_{cy}/σ'_c and the number of load cycles under the constant cyclic frequency f equal to 10 s /cycle to obtain widely various normalized excess pore pressure $\Delta u_{cy}/\sigma'_c$ of 0 through 1.0 generated during cyclic loading.

iii) The double amplitude axial strain ε_{DA} generated during undrained cycling is not large (3.5% at most), but the maximum value of the normalized excess pore pressure becomes nearly 0.9.

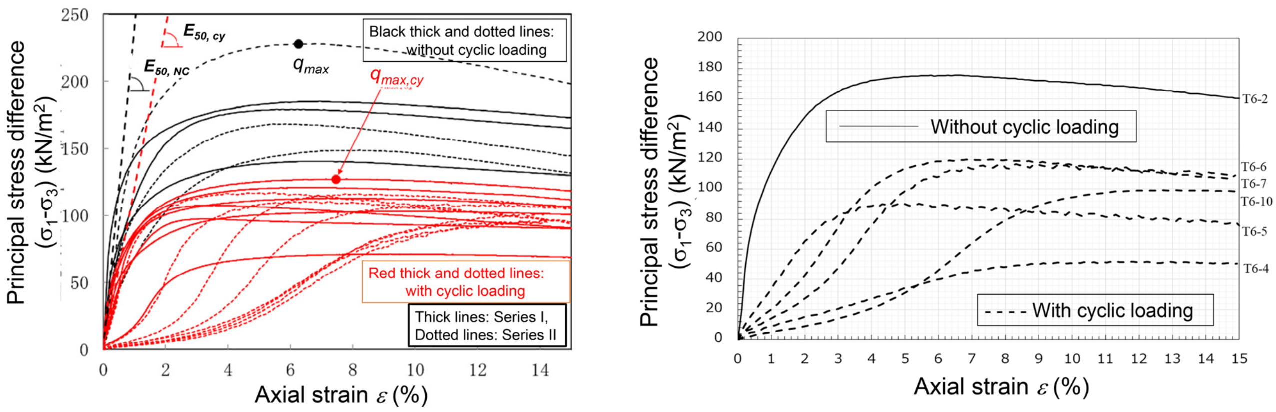

(a) Type I (b) Type II

Fig. 4 – Stress vs. strain relations from post-cyclic undrained triaxial tests

5.2 Determination of strength parameters

Mohr circles were produced in terms of both total and effective stress analysis based on results of post-cyclic undrained triaxial tests. They are depicted for comparison with results from monotonic triaxial tests of undisturbed specimens with no cyclic loading experience under confining pressures of 65, 75, and 90 kPa in Series I. Results portrayed in Figs. 5(a) and 5(b) present a decrease in strength parameters c and ϕ in effective stress analyses. A noteworthy characteristic is that the decrement in cohesion c is almost equal to the decrement in the internal friction angle.

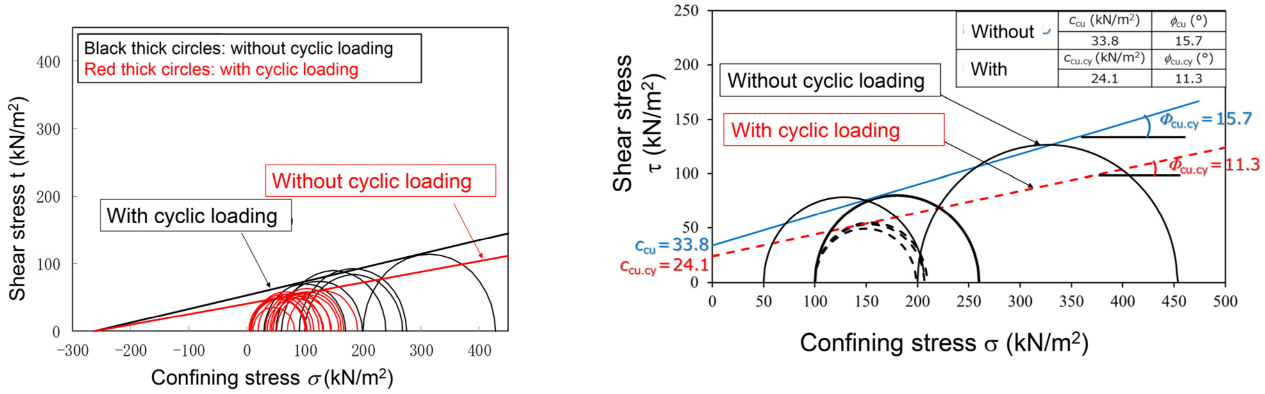

(a) SERIES I and SERIES II (b) SERIES III

Fig. 5 – Mohr circles with envelopes for soils with and without undrained cyclic loading history

5.3 Method for determining strength parameters

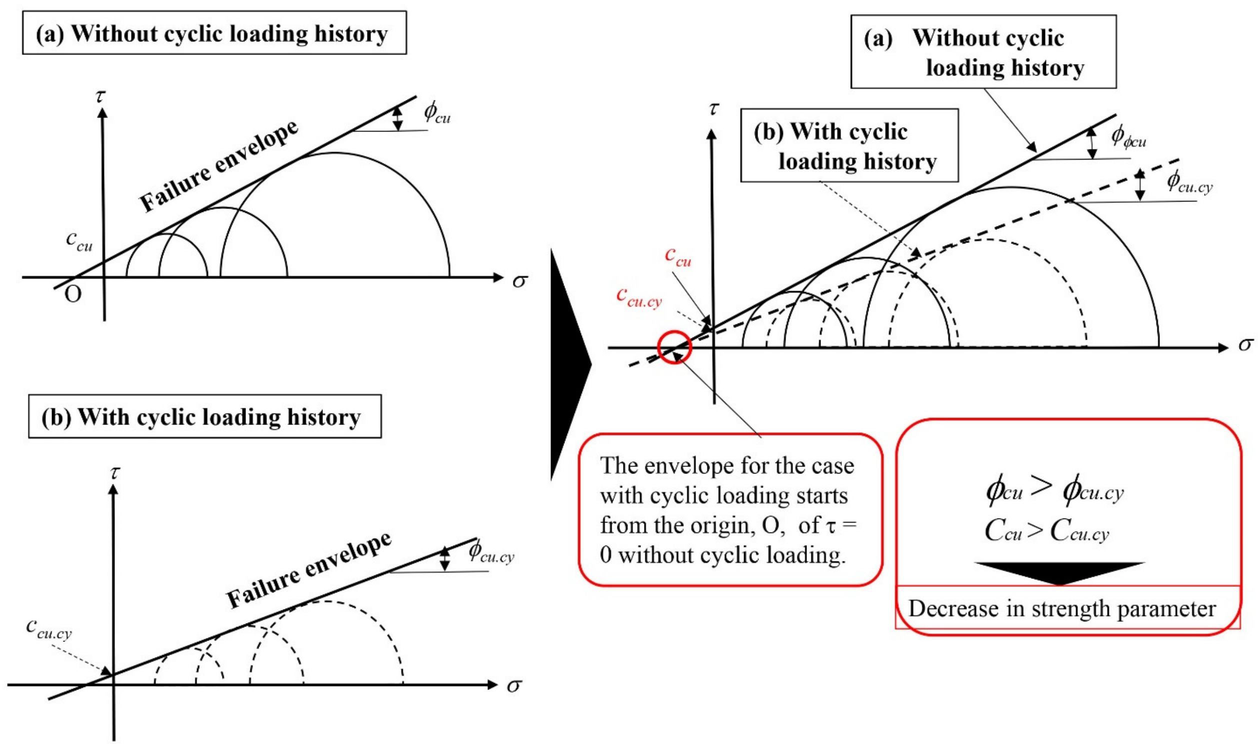

Fig. 6 – Determination of strength constants with and without undrained cyclic loading history

Strength parameters with and without undrained cyclic loading were determined by following the procedure shown in Fig. 6.

i) The envelope for circles without cyclic loading history is drawn with origin t = 0 designated by "O" (see Fig. 6).

ii) The envelope for circles with cyclic loading history is drawn by starting from point O

iii) The intercept of σ = 0 for the envelope with cyclic loading and the gradient of envelope line are designated respectively as $c_{cu,cy}$ and $\phi_{cu,cy}$. They are used for the calculation of residual deformation caused by earthquakes.

Strength parameters determined in terms of total stress analysis using the procedure shown above are presented in Table 4. Apparently, both parameters ϕ_{cu} and c_{cu}, reduce to approximately 70% of the cases without a cyclic loading history.

Table 4 – Change in strength parameters in terms of total stress analysis

	Type-I		Type-II	
	Frictional angle ϕ_{cu} (°)	Cohesion c_{cu} (kN/m^2)	Frictional angle ϕ_{cu} (°)	Cohesion c_{cu} (kN/m^2)
Without cyclic loading	11.5	53.5	15.1	33.8
With cyclic loading	7.7	37.5	11.3	24.1

6. Model for Calculation of Earthquake-Induced Residual Deformation

6.1 Model ground and given seismic acceleration wave

For investigating the influences of GWL, the authors assume the foundation model ground with residences. It consists of two-layered volcanic-ash cohesive soils with the index properties and strength parameters presented in Table 1 and Table 4. The GWL depth is designated by h_w, as is depicted in Fig. 7, which is equivalent to the depth from the ground surface to the GWL.

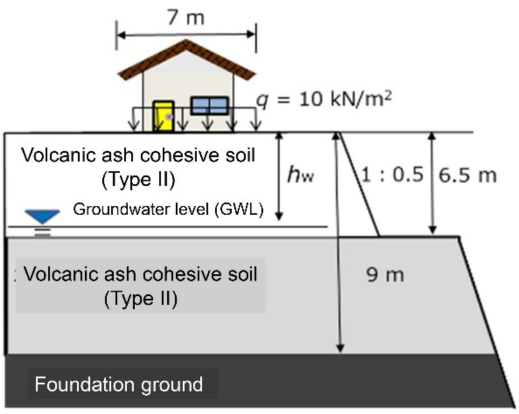

Fig. 7 – Model ground for calculation

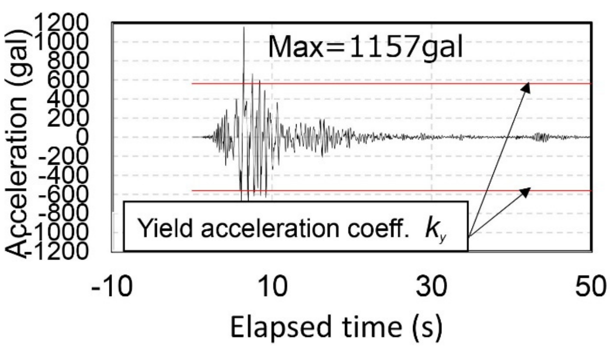

Fig. 8 – Input acceleration wave (after NIED)

Calculation of earthquake-induced residual deformation of foundation grounds used seismic acceleration wave records of measurements taken at the National Research Institute for Earth Science and Disaster Resilience (NIED) station near boring locations in Mashiki Town in Kumamoto (see Fig. 8), which was struck successively by two strong earthquakes in 2016.

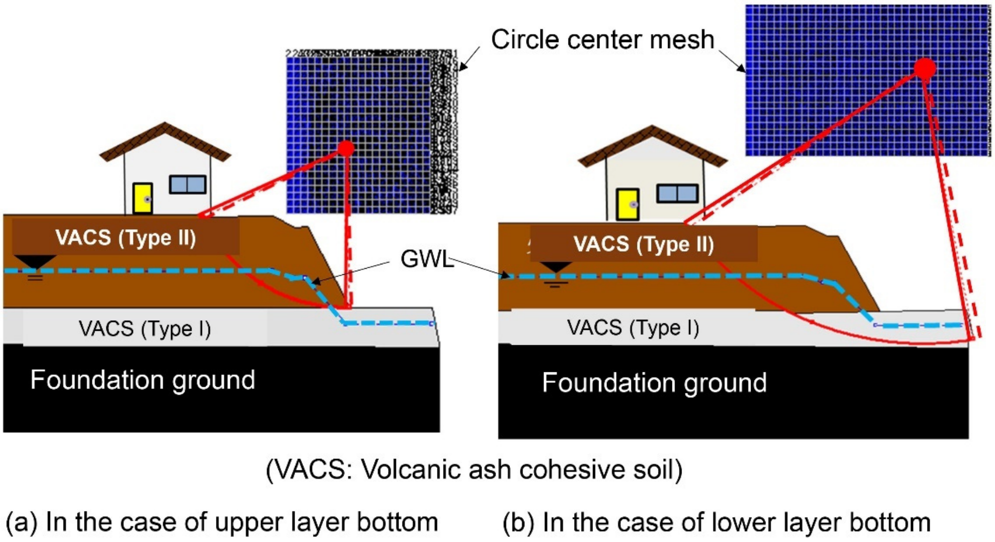

Fig. 9 – Assumed failure circles

Calculations are divided into two cases by assuming the failure circle line passing through the bottoms of the upper layer (CASE 1) and the lower layer (CASE 2), as shown in Fig. 9. Stability analysis is based on the Fellenius method.

6.2 Methodology for estimating the degree of damage to residences

Although a critical value of differential settlement of small-scaled building structures exists for maintaining the function of residences regulated by the Architectural Institute of Japan, this cannot be used for residences subjected to earthquakes. The standardized values of differential settlements and inclination of residences, as presented in Table 5, for estimating the degree of damage to residences caused by earthquakes are regulated by the General Insurance Association of Japan. However, this standard was proposed for evaluating how damaged the residence becomes when undergoing liquefaction. Earthquake-induced settlement is obtained by conversion of residual deformation to the vertical direction.

Table 5 – Regulation for determining the damage condition by General Insurance Association of Japan

Inclination of residence (rad/1000)	Settlement of residence (cm)	Damage condition
3.5–8.7	10–15	Partial failure
8.7–17.5	15–30	Semi-failure
Beyond 17.5	30	Complete failure

The inclination of residences caused by earthquakes is estimated using the following equation.

$$a = \tan^{-1}(\tan^{-1}\frac{\Delta S/_2}{\mathrm{B}}) = \tan^{-1}(\frac{\theta\sqrt{r^2 - {y_0}^2}}{2\mathrm{B}}) \quad (1)$$

In those equations, α denotes the inclination angle (rad), $\otimes S$ represents ground settlement (cm), B signifies the house width (cm), θ is the circle rotational angle (rad), r stands for the failure circle radius (cm), and y_0 denotes the distance from the center of the failure circle to the ground surface (cm).
Eq. (1) is based on the following Fig. 10. The definitions of parameters related to earthquake-induced residual deformation of foundation grounds and residences are presented in Fig. 11.

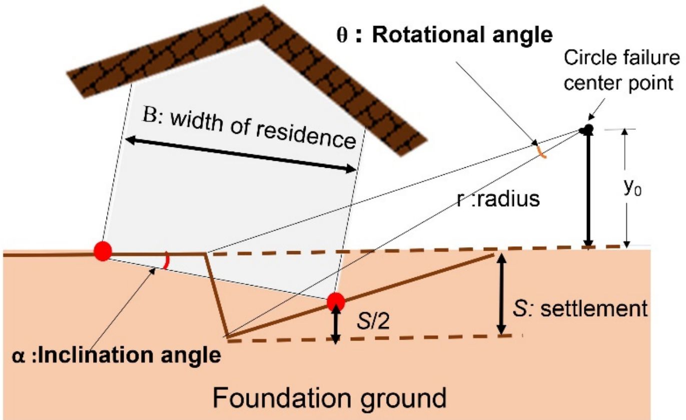

Fig. 10 – Definition of inclination angle

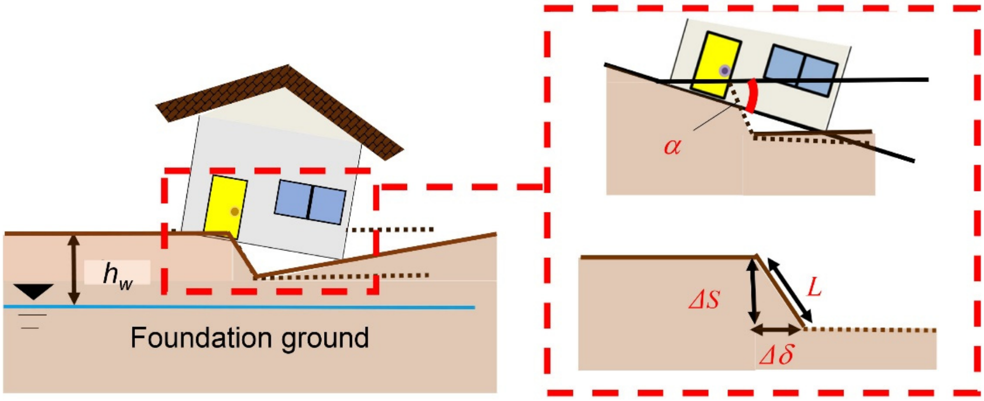

Fig. 11 – Definitions of parameters related to residual deformation

6.3 Residual deformation of residences caused by earthquakes

The results obtained from calculating residual deformation as a set of examples in the case of h_w of 4.0 m in Fig. 7 are presented in Table 6. It is apparent from Table 6 that residual deformation in the case of a large circle failure passing through the bottom of lower layer (CASE 2) is more marked than that in the case of passing through the bottom of the upper layer (CASE 1).

Table 6 – Example of residual deformation of residences caused by earthquakes

(a) CASE 1

Residual deformation L (cm)	Settle-ment ΔS (cm)	Lateral dis-placement $\Delta\delta$ (cm)	Inclination angle α (rad/1000)
23.6	21.5	9.65	15.4

(b) CASE 2

Residual deformation L (cm)	Settle-ment ΔS (cm)	Lateral dis-placement $\Delta\delta$ (cm)	Inclination angle α (rad/1000)
39.2	32.7	21.6	23.4

7. Influence of Groundwater Level (GWL) on Residual Deformation during Earthquake

To evaluate the influences of GWL on earthquake-induced residual deformation for model grounds, calculations were performed for the two cases presented above (CASE 1) and (CASE 2) by varying GWL every 1 m of GWL from 0 m (at the surface) to 9.0 m (at the bottom of foundation ground). Assessment of the influences on residual deformation was done to determine the damage criteria for stability of residences under earthquakes from complete collapse to semi-collapse or partial collapse. These damage criteria are based on the quantitative values of settlement and inclination angle of damaged residences as presented in Table 5 as standardized by the General Insurance Association of Japan for earthquake insurance [10].

The calculated results of earthquake-induced damage are presented in Fig. 12(a) and Fig. 12(b) in the forms of settlement vs. depth of GWL and inclination angle vs. depth of GWL for CASE 1 and CASE 2, respectively. The critical values of settlement and inclination angle taken from Table 5 are drawn as thick horizontal lines in both figures to ascertain the critical values of GWL for avoiding damage to residences.

The results in Fig. 12(a) and Fig. 12(b) clarify that settlement and inclination of residences become greater as GWL increases from the bottom (h_w = 9.0 m) to the surface of foundation grounds (h_w = 0 m). Furthermore, to avoid the complete collapse of residences during earthquakes, results in both Fig. 12(a) and Fig. 12(b) suggest the points enumerated below.

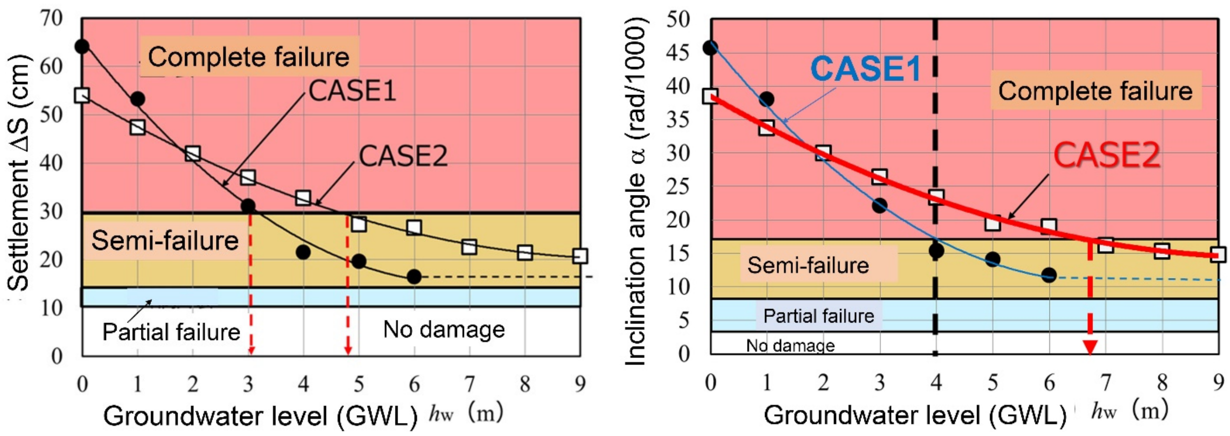

(a) Settlement vs. GWL (b) Inclination angle vs. GWL

Fig. 12 – Determination of damage conditions from settlement and the inclination angle

i) In CASE 1, where the failure circle touches the upper layer surface, the locations of GWL should be kept below 3.0 m to mitigate settlement and below 4.0 m for the inclination angle.

ii) In CASE 2, where the failure circle comes into contact with the lower layer, GWL should be lower, respectively, than 5.0 m and 7.0 m from the surface.

Judging from the results stated above, the authors emphasize the following.

i) Monitoring of GWL is fundamentally important because groundwater is abundant in Kumamoto. For that reason, GWL tends to vary.

ii) Criteria of earthquake-induced allowable settlement and inclination of residences founded on cohesive soil grounds should be regulated following the standards of liquefaction of sand foundation ground.

8. Conclusion

Results of cyclic and post-cyclic triaxial tests of undisturbed volcanic cohesive soils taken from the damage site were used to investigate the influences of GWL on residual deformation using the Newmark method, which probably led to severe damage of residences in Mashiki Town.

The following points were concluded from the investigation described above.

i) The influential degree of GWL on post-earthquake residual deformation is associated with the location at which the slope failure circle reached the bottom of the embankment or foundation ground. Devastating damage to residences at Mashiki Town was probably attributable to the large circle failure passing the bottom of the foundation beneath the residential embankment.

ii) To avoid complete collapse of residences at Mashiki Town during earthquakes, GWL should be lowered to around 7 m from the surface of embankment. This measure can be expected to limit failure of residences to partial failure, not complete failure.

iii) The GWL 4 m from the surface existing at the time the main shock struck Mashiki Town was important, judging from both the amount of settlement and the inclination angle of residences.

iv) Based on the findings stated above, it can be emphasized that monitoring GWL in this area is an important proactive measure for reducing earthquake-induced residual deformation of embankments and foundations.

Acknowledgements

The research described herein was supported financially by a Grant-in-Aid (No.16H02362) from the Ministry of Education, Culture, Sports, Science and Technology (MEXT) to representative Kazuya Yasuhara, Professor Emeritus of Ibaraki University, Japan. NIED kindly permitted the use of acceleration records measured during the Kumamoto earthquake in 2016. The authors express their sincere gratitude for this support and cooperation.

References

[1] Yoshimi M, Goto H, Hata Y, Yoshida N (2017): Nonlinear site response at the worst-hit area of the 2016 Kumamoto earthquakes in Mashiki Town, Kumamoto, Japan. *DPRI Kyoto University Annual Meeting 2017*, A05, (*in Japanese*).

[2] Yasuhara K, Murakami S, Toyota N, Hyde AFL (2001): Settlements in fine-grained soils under cyclic loading. *Soils and Foundations*, **41** (6), 25-36.

[3] Yasuhara K, Hyde AFL, Murakami S (2004): Post-cyclic degradation of saturated plastic silts, *Proc. International Symp. on Cyclic Behaviour of Soils and Liquefaction Phenomena*, Bochum, Germany, 275–286.

[4] Yasuhara K, Watanabe H, Kobayashi K, Yoshimi M, Arai Y, Hosoya S, Tajiri S, Murakami S (2017): Instability of residences founded on volcanic cohesive soils during the 2016 Kumamoto Earthquake. *Lowland Technology International*, **19** (3), 205-216, ISSN 1344-9656.

[5] Yasuhara K, Watanabe M, Kobayashi K, Arai Y, Hyodo M (2019): *Cyclic degradation of volcanic ash cohesive soil strength and stiffness*, Proc. Seventh International Conf. Earthquake Geotechnical Eng., Rome, Italy, 5746-5753, *ISBN 978-0-387-14328-2*.

[6] Tajiri S (2017): Damaged situation of residential area of Mashiki-town, *Proceedings of the International Workshop on the 2016 Kumamoto Earthquake,* pp. 75–84, March 6, Fukuoka, Japan.

[7] Tatsuoka F, Duttine A, Yazaki S, Mohri Y (2014): Evaluation of seismic slip displacement of slope by Newmark method considering soil strength reduction due to undrained cyclic loading and strain-softening. *Proc. Special Symposium of JGS on Overcoming the 2011 Great Tohoku Earthquake* 394–402, (*in Japanese*).

[8] JGS 1997. Testing Methods and Their Interpretation, (*in Japanese*).

[9] Newmark, NM (1968): Effects of earthquakes on dams and embankments. *Gotechnique*, Fifth Rankine Lecture 18: 129–160.

[10] General Insurance Association of Japan: Investigation method in earthquake insurance for building damage cause d by liquefaction http://www.sonpo.or.jp/ news/release/2011/1106_04.html (Browsing in February 1, 2019）.

